

Back to business: SLX 1746–331 after 13 years of silence

JING-QIANG PENG^{*,1,2}, SHU ZHANG^{*,1}, PENG-JU WANG^{*,3}, SHUANG-NAN ZHANG^{1,2}, LING-DA KONG³, YU-PENG CHEN¹,
QING-CANG SHUI^{1,2}, LONG JI⁴, JIN-LU QU¹, LIAN TAO¹, MING-YU GE¹, RUI-CAN MA^{1,2}, ZHI CHANG¹, JIAN LI^{5,6},
ZHAO-SHENG LI⁷, ZHUO-LI YU¹, ZHE YAN^{2,8,9,10}, PENG ZHANG^{11,12}, YUN-XIANG XIAO^{1,2} AND SHU-JIE ZHAO^{1,2}

¹Key Laboratory of Particle Astrophysics, Institute of High Energy Physics, Chinese Academy of Sciences, 100049, Beijing, China

²University of Chinese Academy of Sciences, Chinese Academy of Sciences, 100049, Beijing, China

³Institute für Astronomie und Astrophysik, Kepler Center for Astro and Particle Physics, Eberhard Karls, Universität, Sand 1, D-72076 Tübingen, Germany

⁴School of Physics and Astronomy, Sun Yat-Sen University, Zhuhai, 519082, China

⁵CAS Key Laboratory for Research in Galaxies and Cosmology, Department of Astronomy, University of Science and Technology of China, Hefei 230026, China

⁶School of Astronomy and Space Science, University of Science and Technology of China, Hefei 230026, China

⁷Key Laboratory of Stars and Interstellar Medium, Xiangtan University, Xiangtan 411105, Hunan, China

⁸Yunnan Observatories, Chinese Academy of Sciences, Kunming 650216, China

⁹Key Laboratory for the Structure and Evolution Celestial Objects, Chinese Academy of Sciences, Kunming 650216, China

¹⁰Center for Astronomical Mega-Science, Chinese Academy of Sciences, Beijing 100012, China

¹¹College of Science, China Three Gorges University, Yichang 443002, China

¹²Center for Astronomy and Space Sciences, China Three Gorges University, Yichang 443002, China

ABSTRACT

The black hole candidate system SLX 1746–331 was back to business in 2023, after a long silence of roughly 13 years. An outburst was observed thoroughly by *Insight*-HXMT and *NICER*. The outburst is characterized by spectral dominance of the soft state, where the joint *Insight*-HXMT and *NICER* spectral analysis shows the temperature dependence of the disk flux follows $T_{\text{in}}^{3.98}$, and thus suggests that the inner disk reaches to ISCO during almost the entire outburst. By assuming 0.3 L_{Edd} for the peak flux and an inclination angle of zero degrees, the lower limit of the compact object hosted in this system is estimated as $3.28 \pm 2.14 M_{\odot}$. We also look into the relation of the disk temperature and disk flux for a sample of black hole systems, and by taking the disk temperature derived in the outburst of SLX 1746–331, such a relation results in a mass estimation of $5.2 \pm 4.5 M_{\odot}$. Finally, the spin of the compact object is constrained to larger than 0.8 with a spectral model of kerrbb.

Keywords: X-rays: binaries — X-rays: individual (SLX 1746–331)

1. INTRODUCTION

Low-mass X-ray binaries (LMXBs) consist of a star and a compact star, which is typically a black hole (BH) or a Neutron Star (NS). The typical mass of the companion star in LMXBs is relatively small ($\lesssim 1 M_{\odot}$). The compact object accretes material from the companion star via the Roche-lobe (Shakura & Sunyaev 1973). Some black hole X-ray binaries are known as persistent sources, as they maintain relatively high accretion rates for long periods (Deegan et al. 2009). In contrast, transient sources remain in a quiescent state with a low accretion rate for prolonged periods and are generally challenging to be observed in the X-ray band. When they enter the outburst state, their X-ray emission intensifies and can last from a few days to several months (Cannizzo et al. 1995; Lasota 2001; Belloni et al. 2011; Corral-Santana et al. 2016).

pengjq@ihep.ac.cn

szhang@ihep.ac.cn

wangpj@ihep.ac.cn

For the outbursts of classical black hole X-ray transient sources, their trajectory on the Hardness-Intensity diagram (HID) is so-called "q" shape (Homan et al. 2001; Fender et al. 2004; Motta et al. 2012). Low-mass black hole X-ray binaries can be classified into different spectral states during their outburst cycles, including the Low/Hard States (LHS), High/Soft States (HSS), and Intermediate States (IMS) (Belloni et al. 2005; Motta et al. 2009). In the LHS, the emission is primarily from corona/jet hard X-ray emission, with the non-thermal component dominating and the photon index Γ typically around 1.5. The accretion disk is generally believed to be truncated, with a truncation radius typically greater than $100 R_g$. However, there are some outbursts in which the accretion disk is not truncated in the LHS (Miller et al. 2006; Done & Diaz Trigo 2010). As the luminosity increases, the radius of the disk moves inward, the temperature of the inner disk rises (Gierliński et al. 2008), and the disk reaches its innermost stable circular orbit (ISCO) as it enters into the HSS. At this time, the thermal emission from the disk dominates, and the corona/jet becomes almost invisible with a photon index of about 2.1-3.7 (McClintock & Remillard 2006; Esin et al. 1997). The IMS can be further divided into the hard intermediate state (HIMS) and the soft intermediate state (SIMS), where the energy spectrum of SIMS is softer than that of HIMS (Homan & Belloni 2005).

In a classical successful outburst, a low-mass black hole X-ray binary transfers from the quiescent state to the LHS and then through the IMS to the HSS and back to the LHS as the accretion rate increases, following a counterclockwise "q" shape on the HID (Homan et al. 2001; Homan & Belloni 2005; Belloni & Motta 2016). However, not all outbursts follow a complete "q" shape. In some sources, the accretion rate is so low that the outburst does not reach the HSS but only evolves to the low/hard or intermediate state before ending. These outbursts are known as "failed outbursts" and account for approximately 38% of all outbursts (Brocksopp et al. 2004; Capitanio et al. 2009; Tetarenko et al. 2016). In contrast to the absence of LHS, there is a class of outbursts that do not have a LHS at the beginning of the outburst, or whose LHS is not observed. Such outbursts are relatively rare, as seen in sources like 4U 1630-472 and MAXI J0637-430 (Baby et al. 2020; Ma et al. 2022).

SLX 1746-331 is a transient low-mass X-ray binary located at the galactic center, and was identified within the surveyed fields of the Einstein galactic plane survey conducted by Hertz & Grindlay (1984). It was discovered with the Spacelab 2 XRT in 1985 August and detected by the RASS in 1990 (Warwick et al. 1988; Skinner et al. 1990; Motch et al. 1998; Wilson et al. 2003). SLX 1746-331 had a very soft spectrum, which is best fitted with thermal bremsstrahlung with a temperature of $kT=1.5$ keV. (Skinner et al. 1990) suggested that SLX 1746-331 may be a potential black hole candidate based on its very soft spectrum. In history, outburst of SLX 1746-331 were observed by *RXTE/PCA* (Markwardt & Swank 2007) and *INTEGRAL/JEM-X* in 2007/2008 (Kuulkers et al. 2008) and by *MAXI* in 2010 (Ozawa et al. 2011). Both outbursts exhibited a very soft spectrum and are thought to be associated with black hole candidates (BHCs) in a soft state. Yan & Yu (2015) estimated the distance of SLX 1746-331 to be about 10.81 ± 3.52 kpc using data from *Rossi X-ray Timing Explorer (RXTE)*.

SLX 1746-331 underwent outburst again in 2023 after the long silence of roughly 13 years, and was observed thoroughly by *Insight-HXMT* and *NICER*. SLX 1746-331 was observed a total of 46 times by *Insight-HXMT* over 35 days, from March 14th to April 17th, 2023. And *NICER* conducted 48 observations of SLX 1746-331 over 93 days, from March 8th to June 8th. In this letter, we perform a detailed spectral analysis and reveal some properties regarding both the outburst and the harbored compact object. In Section 2, we describe the observations and data reduction. The detailed results are presented in Section 3. The results are discussed and the conclusions are presented in Section 4.

2. OBSERVATIONS AND DATA REDUCTION

2.1. *Insight-HXMT*

Insight-HXMT is the first Chinese X-ray astronomy satellite, which was successfully launched on 2017 June 15 (Zhang et al. 2014, 2018, 2020). It carries three scientific payloads: the low energy X-ray telescope (LE, SCD detector, 1-15 keV, 384 cm², Chen et al. 2020), the medium energy X-ray telescope (ME, Si-PIN detector, 5-35 keV, 952 cm², Cao et al. 2020), and the high energy X-ray telescope (HE, phoswich NaI(CsI), 20-250 keV, 5100 cm², Liu et al. 2020).

Insight-HXMT started to observe SLX 1746-331 at the peak of its outburst on March 14, 2023 and continued until May 19, 2023. We extract the data from LE and ME using the *Insight-HXMT* Data Analysis software HXMTDAS v2.05. The data are filtered with the criteria recommended of the *Insight-HXMT* Data Reduction Guide v2.05¹ Xspec

¹ <http://hxmtweb.ihep.ac.cn/SoftDoc/648.jhtml>

Table 1. *Insight*-HXMT and *NICER* observations of SLX 1746–331 during the 2023 outburst.

<i>Insight</i> -HXMT	Observed date	LE exposure time	ME exposure time	<i>NICER</i>	Observed date	Exposure Time
ObsID	(MJD)	(s)	(s)	ObsID	(MJD)	(s)
P051436300101	60017.14	1821	2703	6203700101	60011.69	1462
P051436300102	60017.29	260.3	1707	6203700102	60012.02	1932
P051436300103	60017.43	270.3	922.5	6203700103	60013.06	3014
P051436300201	60018.53	1614	2297	6203700104	60014.21	839
P051436300202	60018.71	1822	2947	6203700105	60015.05	766
P051436300301	60020.38	352.1	1949	6203700108	60023.00	1306
P051436300302	60020.56	2633	2678	6203700109	60024.14	2872
P051436300501	60021.38	817	1973	6203700110	60025.30	3888
P051436300502	60021.55	2574	2664	6203700111	60026.08	2212
P051436300601	60022.57	478.8	2178	6203700112	60027.26	724
P051436300602	60022.74	1077	2018	6203700113	60028.46	1838
P051436300603	60022.88	359.1	1079	6203700114	60029.56	2101
P051436300701	60023.56	1937	2650	6203700115	60031.24	1598
P051436300702	60023.74	1137	2020	6203700116	60032.67	1584
P051436300703	60023.87	538.7	1066	6203700117	60039.33	1700
P051436300801	60024.95	1763	2165	6203700118	60043.01	2079
P051436300802	60025.08	955.6	1658	6203700119	60044.03	1831
P051436300803	60025.22	284.3	964.2	6203700120	60046.73	1552
P051436300901	60026.93	2723	3235	6203700121	60047.57	1200
P051436301001	60028.19	627.4	798.9	6203700122	60051.66	1797
P051436301002	60028.34	886.8	2061	6203700123	60052.68	1846
P051436301003	60028.50	119.7	657.4	6203700124	60053.25	1675
P051436301101	60030.04	179.5	1445	6203700125	60054.69	1742
P051436301102	60030.18	579.5	844.2	6203700126	60055.84	1312
P051436301103	60030.32	716.2	1142	6203700127	60056.49	2483
P051436301301	60032.75	718.2	3469	6203700128	60060.68	2297
P051436301302	60032.93	1886	1554	6203700129	60061.65	1227
P051436301303	60033.06	299.2	824	6203700130	60062.48	240
P051436301401	60034.54	1495	3029	6203700131	60063.45	724
P051436301402	60034.72	210.5	3814	6203700132	60064.35	945
P051436301601	60036.32	1915	5360	6203700133	60065.00	275
P051436301801	60040.03	1205	3301	6203700134	60074.12	80
P051436301802	60040.14	770.1	7371	6203700135	60080.30	911
P051436301901	60041.55	1927	5947	6203700136	60081.39	1993
P051436302001	60043.20	3522	4340	6203700137	60082.82	711
P051436302002	60043.44	880.8	1040	6203700138	60083.27	1129
P051436302101	60046.04	2499	2181	6203700139	60084.50	1557
P051436302102	60046.17	1436	1972	6203700140	60085.14	1503
P051436302103	60046.30	1058	1227	6203700141	60086.24	613
P051436302201	60047.83	3711	3709	6203700142	60087.28	52.58
P051436302202	60048.19	3305	3332	6203700143	60088.32	23
P051436302301	60050.08	2503	3064	6203700144	60089.02	770
P051436302302	60050.27	777.1	842.1	6203700145	60089.10	1467
P051436302401	60051.14	2454	2565	6203700146	60093.52	1683
P051436302403	60051.43	1137	996.1	6203700147	60094.76	327
P051436302404	60051.57	2334	2469	6203700148	60096.23	720
				6203700149	60102.81	1410
				6203700150	60103.64	1152

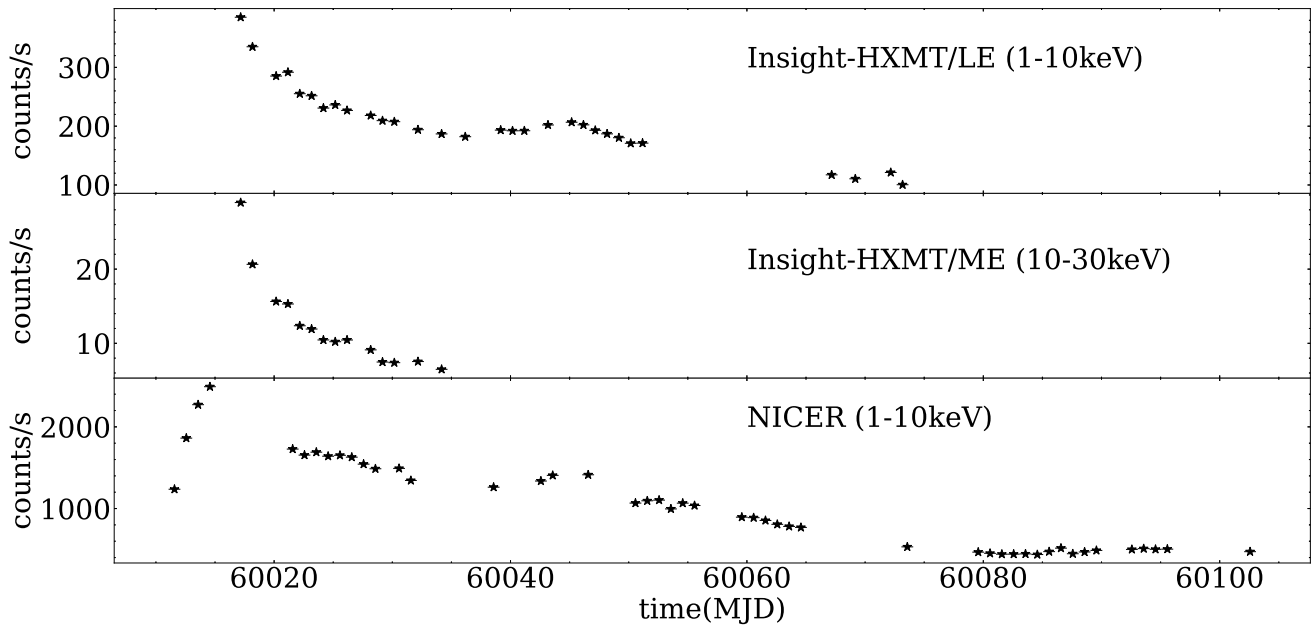


Figure 1. Light curve of SLX 1764–331 during the 2023 outburst. Top panel: the light curve of *Insight*-HXMT LE 1–10 keV Middle panel: the light curve of *Insight*-HXMT ME 10–30 keV Bottom panel: the light curve for *NICER* 1–10 keV.

v12.13.0c² is used to perform analysis of spectrum, where LE data above 2 keV are chosen to suppress possible source pollution at lower energies. Due to the count rate of high-energy photons in SLX 1746–331, the energy bands considered for spectral analysis are LE 2–8 keV and ME 8–25 keV. One percent systematic error is added to data (Liao et al. 2020), and errors are estimated via Markov Chain Monte-Carlo (MCMC) chains with a length of 20000.

2.2. *NICER*

The X-ray Timing Instrument (XTI) of the Neutron Star Interior Composition Explorer (*NICER*) is an International Space Station (ISS) payload, which was launched by the Space X Falcon 9 rocket on 3 June 2017 (Gendreau et al. 2016). And *NICER* has a large effective area and high temporal resolution in soft X-ray band (0.2–12 keV), which may well fit the black body component at low temperatures.

NICER started to observe SLX 1746–331 on March 8, 2023 and continued until June 8, 2023. The *NICER* observations covered the rising phase of the SLX 1746–331 outburst. *NICER* data are reduced using the standard pipeline tool *NICER12*³. We used "overonly_range" and "underonly_range" in the *NICER12* to filter the data. This helped ensure that overshoots (0–1) and undershoots (0–200) were within the recommended range for analysis. We extract light curves using *NICER13-1c*⁴ in 1–4 keV, 4–10 keV and 1–10 keV. We use *NICER13-spect*⁵ to extract the spectrum, with "nibackgen3C50"⁶ model to estimate the background for the spectral analysis. For the fitting of the spectrum, we choose an energy range of 0.5–10 keV.

3. RESULTS

3.1. Light curve and Hardness-intensity diagram

As shown in Figure 1, since the alert from *MAXI* for the outburst of SLX 1746–331, *NICER* observed from March 8 until June 8, covering both the rise and decay phases of the outburst. *Insight*-HXMT observed from the outburst peak on March 14 to the decay phase till May 19 (Table 1).

As *NICER* observations cover the rise and decay of the outburst of SLX 1746–331, we extract the 1–4 keV, 4–10 keV, and 1–10 keV light curves of *NICER* to construct the Hardness-Intensity Diagram (HID) of SLX 1746–331. Figure 2 shows the *NICER* HID of SLX 1746–331 with hardness defined as the count rate ratio of 4–10 keV to 1–4 keV. The red

² <https://heasarc.gsfc.nasa.gov/docs/xanadu/xspec/index.html>

³ <https://heasarc.gsfc.nasa.gov/lheasoft/ftools/headas/NICER12.html>

⁴ <https://heasarc.gsfc.nasa.gov/docs/software/lheasoft/ftools/headas/NICER13-1c.html>

⁵ <https://heasarc.gsfc.nasa.gov/docs/software/lheasoft/help/NICER13-spect.html>

⁶ https://heasarc.gsfc.nasa.gov/docs/NICER/analysis_threads/background/

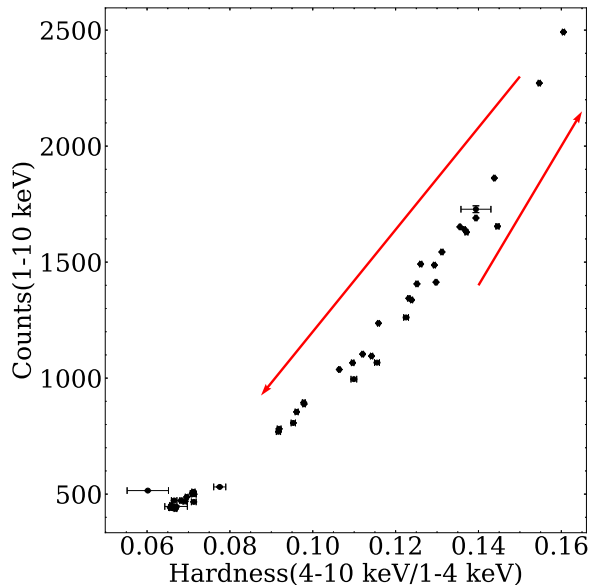


Figure 2. The *NICER* hardness-intensity diagram of SLX 1746–331, where the hardness is defined as the ratio of 4–10 keV to 1–4 keV count rate. The red arrows represent the direction of the evolution.

arrows in the HID represent the trajectory of SLX 1746–331, where it is observed that the outburst of SLX 1746–331 begins in a soft state, then slightly hardens, and eventually evolves toward softer.

We use the tool `powspec`⁷ of `HEASOFT` to generate power spectra with a time resolution of 0.008 s, the interval of 65.5 s and Nyquist frequency of 62.5 Hz, under the Miyamoto normalization (Belloni & Hasinger 1990; Miyamoto et al. 1992). Only a very weak power-law noise is visible in the power density spectrum (PDS), and no QPO is detected. These indicate that it remains in a soft state throughout the outburst.

3.2. Evolution of the Spectral parameters

We use 0.5–10 keV *NICER* data for spectral analysis of SLX 1746–331 during the 2023 outburst. The first trial for the spectral model (M1) is `TBABS*DISKBB`, where `TBABS` accounts for the interstellar absorption (Wilms et al. 2000) by considering photoelectric cross-sections provided by Verner et al. (1996) and `DISKBB` for the multi-temperature blackbody of the accretion disk (Mitsuda et al. 1984). M1 model results in an acceptable fit, with $\chi^2/(\text{d.o.f})=142.75/152=0.94$.

The flux of the disk in the 1–100 keV is estimated with `CFLUX`. As shown in the left panel of Figure 3, the interstellar absorption remains stable at around $0.64^{+0.02}_{-0.02} \times 10^{22} \text{ cm}^{-2}$ and the normalization of the disk is around 70, indicating that the inner radius of the disk is relatively stable. The inner disk temperature (T_{in}) initially increases and then decreases. The disk flux versus the inner disk temperature (T_{in}) is plotted in Figure 4, and a fit with power law results in α around 3.980 ± 0.004 . This finding suggests that the disk is at the innermost stable circular orbit (ISCO) during the whole outburst. We also fit the spectrum of *Insight*-HXMT with M1. Because of the calibration problem of LE, we ignore energies below 2 keV. Accordingly, the column density N_{H} can not be well constrained and hence fixed at $0.64 \times 10^{22} \text{ cm}^{-2}$ and we multiply a `CONSTANT` component to account for the calibration discrepancies between *Insight*-HXMT LE and ME (in this paper, we fix the constant of LE to 1). At this step, an obvious Compton hump shows up in the residual [$\chi^2/(\text{d.o.f})=1141.87/325=3.5$]. So we add a powerlaw component to fit this residual [$\chi^2/(\text{d.o.f})=256.11/323=0.79$]. Therefore, the alternative fitting model (M2) is `CONSTANT*TBABS*(DISKBB+POWERLAW)`. The evolution of the spectral parameters is presented in the right panel of Figure 3. We find in Figure 3 that, while the evolution of the disk component remains almost the same as M1, the normalization of `POWERLAW` and the photon index Γ decrease over time.

3.3. Properties of the system and the compact object

⁷ <https://heasarc.gsfc.nasa.gov/docs/xanadu/xronos/examples/powspec.html>

Table 2. Fitting results of *NICER* for Model M1. N_{H} is the interstellar absorption, T_{in} is the inner disk temperature, Norm(disk) is the normalization of the disk, and Flux is the flux of the unabsorbed disk from 1 to 100 keV.

<i>NICER</i> ObsID	N_{H} 10^{22} cm^{-2}	T_{in} (keV)	Norm(disk)	Flux $10^{-8} \text{ erg s}^{-1} \text{ cm}^{-2}$	χ^2/dof
6203700101	$0.63^{+0.005}_{-0.004}$	$1.51^{+0.01}_{-0.01}$	$70.8^{+1.4}_{-1.3}$	$0.65^{+0.002}_{-0.002}$	279.96/142
6203700102	$0.65^{+0.003}_{-0.003}$	$1.70^{+0.01}_{-0.01}$	$67.3^{+1.1}_{-1.1}$	$1.04^{+0.004}_{-0.003}$	172.11/148
6203700103	$0.66^{+0.003}_{-0.002}$	$1.79^{+0.01}_{-0.01}$	$70.6^{+1.0}_{-1.0}$	$1.38^{+0.006}_{-0.002}$	229.20/153
6203700104	$0.66^{+0.003}_{-0.003}$	$1.92^{+0.01}_{-0.01}$	$68.5^{+1.2}_{-1.2}$	$1.79^{+0.004}_{-0.011}$	170.92/146
6203700105	$0.66^{+0.003}_{-0.003}$	$1.91^{+0.01}_{-0.01}$	$69.9^{+1.2}_{-1.2}$	$1.77^{+0.011}_{-0.002}$	170.09/147
6203700108	$0.64^{+0.003}_{-0.003}$	$1.77^{+0.01}_{-0.01}$	$69.0^{+1.1}_{-1.0}$	$1.09^{+0.005}_{-0.003}$	189.56/149
6203700109	$0.65^{+0.003}_{-0.003}$	$1.70^{+0.01}_{-0.01}$	$67.5^{+1.0}_{-1.1}$	$1.05^{+0.002}_{-0.005}$	172.98/152
6203700110	$0.65^{+0.004}_{-0.004}$	$1.68^{+0.01}_{-0.01}$	$68.9^{+1.0}_{-1.0}$	$1.02^{+0.006}_{-0.001}$	172.48/152
6203700111	$0.65^{+0.003}_{-0.003}$	$1.67^{+0.01}_{-0.01}$	$68.3^{+1.1}_{-1.1}$	$0.99^{+0.005}_{-0.009}$	202.59/152
6203700112	$0.65^{+0.004}_{-0.004}$	$1.68^{+0.01}_{-0.01}$	$67.8^{+1.4}_{-1.3}$	$1.02^{+0.009}_{-0.011}$	138.41/143
6203700113	$0.65^{+0.003}_{-0.003}$	$1.64^{+0.01}_{-0.01}$	$69.1^{+1.0}_{-1.1}$	$0.92^{+0.002}_{-0.004}$	165.74/151
6203700114	$0.65^{+0.004}_{-0.004}$	$1.62^{+0.01}_{-0.01}$	$69.7^{+1.1}_{-1.1}$	$0.90^{+0.001}_{-0.005}$	184.06/151
6203700115	$0.65^{+0.004}_{-0.004}$	$1.60^{+0.01}_{-0.01}$	$71.6^{+1.2}_{-1.2}$	$0.85^{+0.007}_{-0.002}$	168.58/149
6203700116	$0.64^{+0.004}_{-0.004}$	$1.57^{+0.01}_{-0.01}$	$70.4^{+1.2}_{-1.2}$	$0.79^{+0.003}_{-0.006}$	167.93/149
6203700117	$0.63^{+0.005}_{-0.005}$	$1.58^{+0.01}_{-0.01}$	$65.1^{+1.5}_{-1.5}$	$0.75^{+0.004}_{-0.003}$	131.17/135
6203700118	$0.64^{+0.003}_{-0.003}$	$1.60^{+0.01}_{-0.01}$	$65.9^{+1.0}_{-1.0}$	$0.77^{+0.006}_{-0.002}$	172.50/150
6203700119	$0.64^{+0.003}_{-0.003}$	$1.59^{+0.01}_{-0.01}$	$67.4^{+1.1}_{-1.1}$	$0.80^{+0.004}_{-0.004}$	177.61/150
6203700120	$0.64^{+0.003}_{-0.003}$	$1.57^{+0.01}_{-0.01}$	$72.5^{+1.2}_{-1.2}$	$0.81^{+0.006}_{-0.002}$	178.51/152
6203700121	$0.64^{+0.004}_{-0.003}$	$1.56^{+0.01}_{-0.01}$	$69.2^{+1.2}_{-1.2}$	$0.74^{+0.004}_{-0.003}$	148.69/145
6203700122	$0.63^{+0.004}_{-0.003}$	$1.51^{+0.01}_{-0.01}$	$66.6^{+1.1}_{-1.1}$	$0.63^{+0.003}_{-0.005}$	158.54/145
6203700123	$0.63^{+0.004}_{-0.003}$	$1.49^{+0.01}_{-0.01}$	$67.3^{+1.1}_{-1.1}$	$0.61^{+0.003}_{-0.005}$	153.22/145
6203700124	$0.64^{+0.004}_{-0.003}$	$1.48^{+0.01}_{-0.01}$	$68.9^{+1.1}_{-1.1}$	$0.60^{+0.002}_{-0.003}$	164.67/145
6203700125	$0.64^{+0.003}_{-0.003}$	$1.45^{+0.01}_{-0.01}$	$70.0^{+1.2}_{-1.2}$	$0.57^{+0.003}_{-0.002}$	151.27/145
6203700126	$0.64^{+0.003}_{-0.003}$	$1.44^{+0.01}_{-0.01}$	$69.9^{+1.2}_{-1.2}$	$0.54^{+0.005}_{-0.002}$	172.30/141
6203700127	$0.64^{+0.003}_{-0.003}$	$1.43^{+0.01}_{-0.01}$	$71.8^{+1.1}_{-1.1}$	$0.54^{+0.002}_{-0.002}$	213.12/180
6203700128	$0.64^{+0.003}_{-0.003}$	$1.36^{+0.01}_{-0.01}$	$73.8^{+1.2}_{-1.2}$	$0.50^{+0.012}_{-0.006}$	177.31/144
6203700129	$0.64^{+0.004}_{-0.004}$	$1.34^{+0.01}_{-0.01}$	$74.0^{+1.4}_{-1.4}$	$0.43^{+0.002}_{-0.001}$	156.15/140
6203700130	$0.63^{+0.006}_{-0.006}$	$1.35^{+0.01}_{-0.01}$	$71.3^{+2.4}_{-2.3}$	$0.42^{+0.002}_{-0.004}$	154.03/125
6203700131	$0.64^{+0.005}_{-0.005}$	$1.34^{+0.01}_{-0.01}$	$73.1^{+1.8}_{-1.8}$	$0.41^{+0.003}_{-0.005}$	177.01/134
6203700132	$0.63^{+0.004}_{-0.004}$	$1.31^{+0.01}_{-0.01}$	$73.6^{+1.6}_{-1.5}$	$0.39^{+0.002}_{-0.001}$	166.93/136
6203700133	$0.63^{+0.006}_{-0.006}$	$1.31^{+0.01}_{-0.01}$	$73.7^{+2.4}_{-2.3}$	$0.38^{+0.003}_{-0.001}$	139.89/125
6203700134	$0.63^{+0.005}_{-0.005}$	$1.17^{+0.02}_{-0.02}$	$73.3^{+2.3}_{-2.0}$	$0.26^{+0.004}_{-0.003}$	139.03/103
6203700135	$0.62^{+0.005}_{-0.005}$	$1.13^{+0.01}_{-0.01}$	$76.5^{+2.0}_{-1.9}$	$0.21^{+0.002}_{-0.001}$	189.92/131
6203700136	$0.62^{+0.005}_{-0.005}$	$1.12^{+0.01}_{-0.01}$	$76.5^{+2.0}_{-1.9}$	$0.20^{+0.002}_{-0.002}$	171.71/136
6203700137	$0.63^{+0.004}_{-0.004}$	$1.11^{+0.01}_{-0.01}$	$77.1^{+1.6}_{-1.6}$	$0.19^{+0.001}_{-0.001}$	151.01/126
6203700138	$0.63^{+0.005}_{-0.005}$	$1.10^{+0.01}_{-0.01}$	$79.4^{+2.3}_{-2.2}$	$0.19^{+0.003}_{-0.002}$	146.92/131
6203700139	$0.62^{+0.005}_{-0.005}$	$1.10^{+0.01}_{-0.01}$	$77.8^{+2.0}_{-1.9}$	$0.19^{+0.002}_{-0.002}$	172.00/135
6203700140	$0.62^{+0.005}_{-0.004}$	$1.12^{+0.01}_{-0.01}$	$73.6^{+1.7}_{-1.7}$	$0.19^{+0.002}_{-0.001}$	150.89/134
6203700141	$0.62^{+0.005}_{-0.005}$	$1.12^{+0.01}_{-0.01}$	$74.5^{+1.8}_{-1.7}$	$0.19^{+0.002}_{-0.001}$	127.04/109
6203700144	$0.63^{+0.005}_{-0.005}$	$1.13^{+0.01}_{-0.01}$	$78.2^{+2.1}_{-2.0}$	$0.21^{+0.002}_{-0.002}$	142.64/127
6203700145	$0.63^{+0.004}_{-0.004}$	$1.14^{+0.01}_{-0.01}$	$76.7^{+1.7}_{-1.7}$	$0.21^{+0.002}_{-0.002}$	154.44/137
6203700146	$0.63^{+0.004}_{-0.004}$	$1.15^{+0.01}_{-0.01}$	$76.2^{+1.6}_{-1.6}$	$0.23^{+0.001}_{-0.001}$	158.31/137
6203700147	$0.63^{+0.007}_{-0.007}$	$1.14^{+0.01}_{-0.01}$	$79.82^{+2.9}_{-2.8}$	$0.23^{+0.004}_{-0.002}$	112.28/120
6203700148	$0.63^{+0.005}_{-0.005}$	$1.15^{+0.01}_{-0.01}$	$78.46^{+2.2}_{-2.1}$	$0.23^{+0.003}_{-0.002}$	157.26/128
6203700149	$0.62^{+0.005}_{-0.005}$	$1.13^{+0.01}_{-0.01}$	$76.7^{+1.8}_{-1.7}$	$0.21^{+0.002}_{-0.001}$	171.09/134
6203700150	$0.62^{+0.005}_{-0.005}$	$1.13^{+0.01}_{-0.01}$	$75.6^{+1.9}_{-1.8}$	$0.20^{+0.002}_{-0.001}$	161.08/132

Table 3. Fitting results of *Insight*-HXMT for Model M2. T_{in} is the inner disk temperature, Norm(disk) is the normalisation of the disk, Γ is the photon index, and Norm(powerlaw) is the normalisation of the powerlaw component.

<i>Insight</i> -HXMT ObsID	T_{in} (keV)	Norm(disk)	Γ	Norm(powerlaw)	χ^2/dof
P051436300101	1.78 ^{+0.01} _{-0.01}	83.5 ^{+2.88} _{-3.0}	2.09 ^{+0.08} _{-0.10}	0.51 ^{+0.13} _{-0.13}	256.11/323
P051436300102	1.86 ^{+0.02} _{-0.02}	67.2 ^{+2.10} _{-3.80}	2.10 ^{+0.12} _{-0.13}	0.52 ^{+0.19} _{-0.16}	253.43/323
P051436300103	1.78 ^{+0.02} _{-0.02}	82.9 ^{+3.8} _{-4.7}	2.03 ^{+0.17} _{-0.27}	0.35 ^{+0.22} _{-0.20}	309.36/323
P051436300201	1.75 ^{+0.01} _{-0.01}	81.2 ^{+2.7} _{-2.7}	2.13 ^{+0.10} _{-0.13}	0.37 ^{+0.12} _{-0.12}	238.04/323
P051436300202	1.72 ^{+0.01} _{-0.01}	80.9 ^{+2.2} _{-2.5}	2.02 ^{+0.12} _{-0.11}	0.27 ^{+0.10} _{-0.07}	236.79/323
P051436300301	1.75 ^{+0.02} _{-0.02}	67.6 ^{+4.5} _{-4.7}	2.28 ^{+0.18} _{-0.27}	0.39 ^{+0.24} _{-0.20}	273.27/323
P051436300302	1.68 ^{+0.01} _{-0.01}	78.3 ^{+2.2} _{-2.7}	1.96 ^{+0.14} _{-0.15}	0.19 ^{+0.09} _{-0.06}	247.27/323
P051436300501	1.73 ^{+0.03} _{-0.02}	70.3 ^{+3.8} _{-4.7}	2.18 ^{+0.18} _{-0.17}	0.35 ^{+0.23} _{-0.13}	251.18/323
P051436300502	1.67 ^{+0.01} _{-0.01}	80.3 ^{+2.1} _{-2.8}	1.95 ^{+0.14} _{-0.17}	0.19 ^{+0.10} _{-0.08}	259.19/323
P051436300601	1.67 ^{+0.02} _{-0.02}	73.4 ^{+3.3} _{-5.1}	2.07 ^{+0.26} _{-0.20}	0.23 ^{+0.24} _{-0.10}	245.89/323
P051436300602	1.64 ^{+0.01} _{-0.01}	78.4 ^{+2.5} _{-3.5}	1.95 ^{+0.21} _{-0.15}	0.15 ^{+0.12} _{-0.05}	263.53/323
P051436300603	1.66 ^{+0.02} _{-0.02}	69.6 ^{+5.4} _{-4.5}	2.39 ^{+0.15} _{-0.20}	0.44 ^{+0.20} _{-0.20}	278.92/323
P051436300701	1.62 ^{+0.01} _{-0.01}	77.5 ^{+2.2} _{-3.5}	1.86 ^{+0.25} _{-0.17}	0.22 ^{+0.14} _{-0.05}	251.14/323
P051436300702	1.64 ^{+0.02} _{-0.01}	73.7 ^{+3.7} _{-4.4}	2.25 ^{+0.19} _{-0.19}	0.29 ^{+0.18} _{-0.12}	243.51/323
P051436300703	1.63 ^{+0.02} _{-0.01}	76.3 ^{+3.7} _{-4.7}	1.96 ^{+0.30} _{-0.35}	0.15 ^{+0.20} _{-0.09}	256.22/323
P051436300801	1.58 ^{+0.01} _{-0.01}	84.6 ^{+2.2} _{-4.1}	2.14 ^{+0.12} _{-0.12}	0.21 ^{+0.16} _{-0.06}	243.52/323
P051436300802	1.61 ^{+0.02} _{-0.01}	75.9 ^{+4.2} _{-4.5}	2.28 ^{+0.15} _{-0.20}	0.34 ^{+0.17} _{-0.14}	256.91/323
P051436300803	1.60 ^{+0.03} _{-0.02}	79.2 ^{+4.6} _{-7.68}	2.27 ^{+0.35} _{-0.22}	0.23 ^{+0.33} _{-0.11}	242.56/323
P051436300901	1.55 ^{+0.01} _{-0.01}	86.7 ^{+2.6} _{-3.7}	2.20 ^{+0.13} _{-0.12}	0.30 ^{+0.13} _{-0.08}	243.46/323
P051436301001	1.50 ^{+0.02} _{-0.01}	96.5 ^{+3.9} _{-6.7}	2.04 ^{+0.30} _{-0.23}	0.16 ^{+0.20} _{-0.08}	283.36/323
P051436301002	1.69 ^{+0.03} _{-0.02}	54.3 ^{+4.5} _{-4.9}	2.47 ^{+0.14} _{-0.15}	0.64 ^{+0.26} _{-0.20}	284.50/323
P051436301003	1.54 ^{+0.04} _{-0.02}	81.1 ^{+4.4} _{-6.1}	2.00 ^{+0.46} _{-0.30}	0.16 ^{+0.44} _{-0.09}	251.22/323
P051436301101	1.57 ^{+0.04} _{-0.02}	71.6 ^{+5.39} _{-8.5}	2.36 ^{+0.26} _{-0.18}	0.38 ^{+0.35} _{-0.15}	268.59/323
P051436301102	1.52 ^{+0.01} _{-0.02}	86.9 ^{+3.70} _{-3.80}	2.29 ^{+0.15} _{-0.22}	0.26 ^{+0.08} _{-0.01}	228.04/323
P051436301103	1.53 ^{+0.02} _{-0.02}	79.9 ^{+6.12} _{-6.31}	2.17 ^{+0.23} _{-0.37}	0.23 ^{+0.20} _{-0.15}	231.82/323
P051436301301	1.51 ^{+0.01} _{-0.01}	84.1 ^{+2.61} _{-3.60}	1.67 ^{+0.26} _{-0.21}	0.16 ^{+0.07} _{-0.03}	263.65/323
P051436301302	1.50 ^{+0.01} _{-0.01}	83.18 ^{+3.86} _{-4.35}	2.01 ^{+0.23} _{-0.25}	0.15 ^{+0.14} _{-0.07}	218.54/323
P051436301303	1.47 ^{+0.02} _{-0.01}	90.71 ^{+4.55} _{-7.15}	1.87 ^{+0.30} _{-0.30}	0.12 ^{+0.16} _{-0.07}	266.04/323
P051436301401	1.51 ^{+0.01} _{-0.01}	76.5 ^{+3.5} _{-3.8}	2.07 ^{+0.20} _{-0.32}	0.15 ^{+0.15} _{-0.07}	268.30/323
P051436301402	1.49 ^{+0.02} _{-0.02}	81.1 ^{+5.6} _{-5.2}	2.06 ^{+0.24} _{-0.25}	0.15 ^{+0.12} _{-0.08}	287.45/323
P051436301601	1.50 ^{+0.01} _{-0.01}	75.82 ^{+3.1} _{-2.9}	2.17 ^{+0.12} _{-0.15}	0.22 ^{+0.09} _{-0.07}	266.66/323
P051436301801	1.50 ^{+0.02} _{-0.01}	80.8 ^{+2.6} _{-4.6}	2.05 ^{+0.22} _{-0.19}	0.16 ^{+0.12} _{-0.06}	236.00/323
P051436301802	1.51 ^{+0.02} _{-0.01}	77.5 ^{+3.3} _{-4.5}	2.22 ^{+0.17} _{-0.15}	0.24 ^{+0.14} _{-0.09}	283.88/323
P051436301901	1.51 ^{+0.01} _{-0.01}	81.0 ^{+1.9} _{-4.0}	2.01 ^{+0.20} _{-0.12}	0.13 ^{+0.10} _{-0.04}	269.31/323
P051436302001	1.50 ^{+0.01} _{-0.01}	83.8 ^{+2.12} _{-3.36}	2.01 ^{+0.28} _{-0.20}	0.14 ^{+0.09} _{-0.06}	232.00/323
P051436302002	1.53 ^{+0.02} _{-0.01}	76.2 ^{+3.5} _{-5.9}	2.36 ^{+0.20} _{-0.15}	0.30 ^{+0.20} _{-0.10}	239.24/323
P051436302101	1.49 ^{+0.01} _{-0.01}	93.7 ^{+2.3} _{-3.3}	1.99 ^{+0.18} _{-0.13}	0.17 ^{+0.11} _{-0.05}	233.56/323
P051436302102	1.48 ^{+0.01} _{-0.01}	93.8 ^{+2.3} _{-4.5}	1.99 ^{+0.18} _{-0.13}	0.16 ^{+0.11} _{-0.05}	254.91/323
P051436302103	1.48 ^{+0.01} _{-0.01}	94.3 ^{+3.7} _{-5.9}	2.04 ^{+0.20} _{-0.18}	0.23 ^{+0.18} _{-0.09}	265.15/323
P051436302201	1.45 ^{+0.01} _{-0.01}	95.6 ^{+2.7} _{-3.3}	1.99 ^{+0.18} _{-0.17}	0.13 ^{+0.11} _{-0.05}	244.50/323
P051436302202	1.45 ^{+0.01} _{-0.01}	95.0 ^{+2.4} _{-2.9}	1.76 ^{+0.17} _{-0.20}	0.07 ^{+0.03} _{-0.08}	223.11/323
P051436302301	1.44 ^{+0.01} _{-0.01}	93.1 ^{+2.1} _{-3.1}	1.64 ^{+0.25} _{-0.25}	0.06 ^{+0.05} _{-0.03}	220.24/323
P051436302302	1.43 ^{+0.01} _{-0.01}	96.3 ^{+3.7} _{-3.2}	1.13 ^{+0.39} _{-0.20}	0.02 ^{+0.04} _{-0.01}	246.93/323
P051436302401	1.43 ^{+0.01} _{-0.01}	87.3 ^{+2.7} _{-4.3}	1.91 ^{+0.24} _{-0.25}	0.12 ^{+0.12} _{-0.06}	203.96/323
P051436302403	1.43 ^{+0.01} _{-0.01}	89.7 ^{+2.4} _{-4.5}	1.55 ^{+0.51} _{-0.40}	0.03 ^{+0.11} _{-0.02}	260.75/323
P051436302404	1.43 ^{+0.01} _{-0.01}	88.3 ^{+3.4} _{-5.4}	2.03 ^{+0.26} _{-0.24}	0.15 ^{+0.16} _{-0.07}	218.42/323

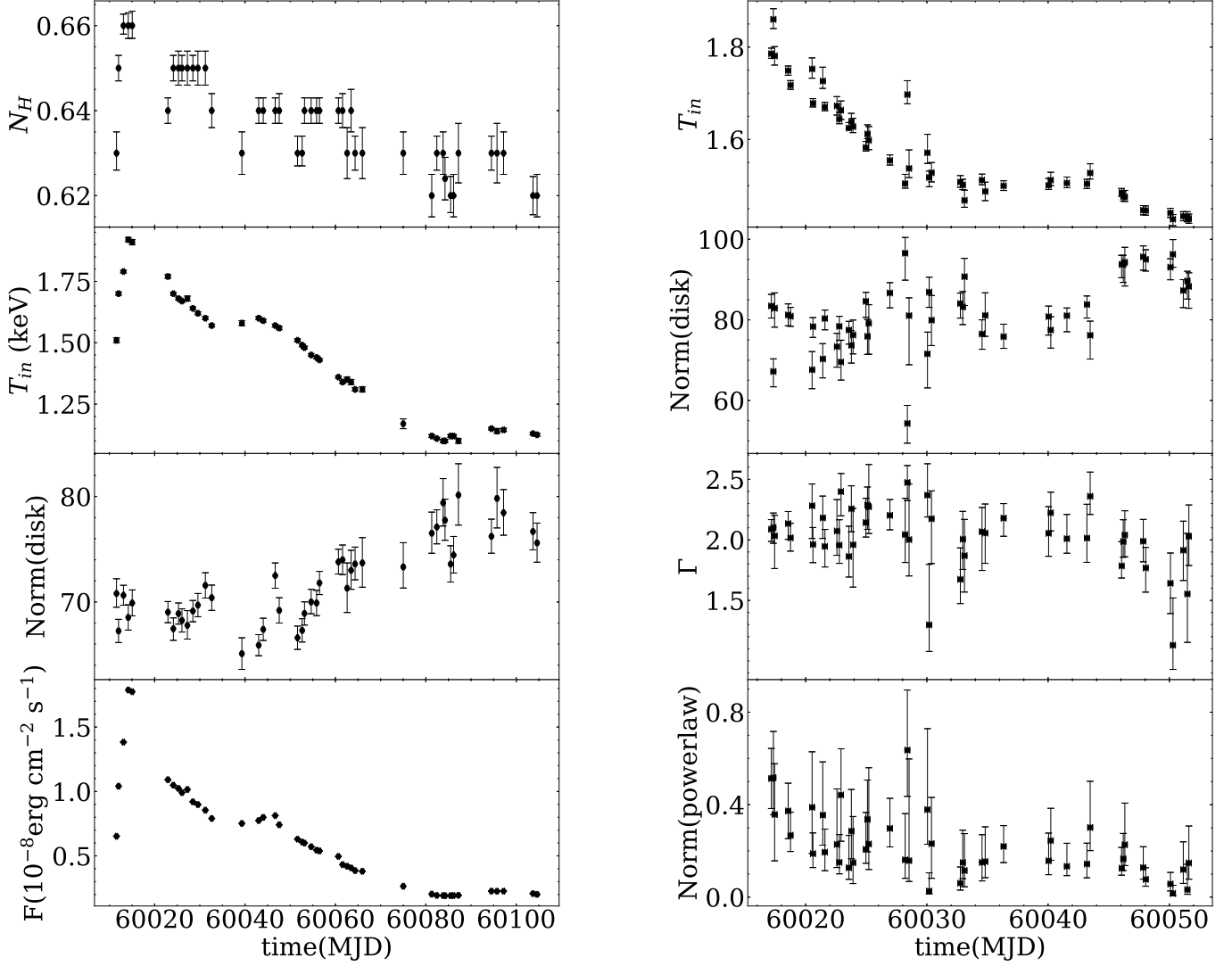


Figure 3. Left panel: Evolution of the spectral parameters by the fitting of *NICER* with M1. N_H is the interstellar absorption, T_{in} is the inner disk temperature, Norm(disk) is the normalization of the disk, and F is the flux of the unabsorbed disk from 1 to 100 keV. Right panel: Evolution of the spectral parameters by the fitting of *Insigh-HXMT* with M2. T_{in} is the inner disk temperature, Norm(disk) is the normalisation of the disk, Γ is the photon index, and Norm(powerlaw) is the normalisation of the powerlaw component.

As shown in Figure 4, we use M1 to fit the spectrum and obtain a flux of the disk that is proportional to the fourth power of the temperature of the inner disk. For the standard thin disk, $L_{\text{disk}} \approx 4\pi R_{\text{in}}^2 \sigma T_{\text{in}}^4$, with R_{in} , T_{in} , and σ representing the inner radius, the temperature of the disk and Stefan-Boltzmann constant respectively. This indicates that the disk is at the ISCO, and the standard disk applies to a luminosity range of $0.001 L_{\text{Edd}} \lesssim L_{\text{disk}} \lesssim 0.3 L_{\text{Edd}}$ (Steiner et al. 2010; Salvesen et al. 2013; García et al. 2015; Draghis et al. 2023), where L_{Edd} is the Eddington luminosity ($L_{\text{Edd}} = 1.26 \times 10^{38} \left(\frac{M}{M_{\odot}}\right)$ erg/s). As shown in Figure 4, we find that the maximum flux for the disk is about ten times greater than the lowest flux. If we assume that the peak flux has reached a value around $0.3 L_{\text{Edd}}$, we can use the flux and luminosity conversion in X-ray binaries to estimate the mass of the compact object. For a disk blackbody emission, the luminosity of the disk can be approximated as $L_{\text{disk}} \approx \frac{2\pi F d^2}{\cos\theta}$, where the distance $d = 10.81 \pm 3.52$ kpc (Yan & Yu 2015), and thus a peak luminosity is $L_{\text{disk}} = \frac{1.24 \pm 0.81 \times 10^{38}}{\cos\theta}$ erg/s. By taking $\theta = 0$, we can estimate a lower mass limit of the compact object $M \geq 3.28 \pm 2.14 M_{\odot}$.

We also take an alternative approach to investigate the possible mass of the compact object hosted in SLX 1736–331. As shown in Table 4, we constitute a sample by selecting in literature the black hole systems with measured

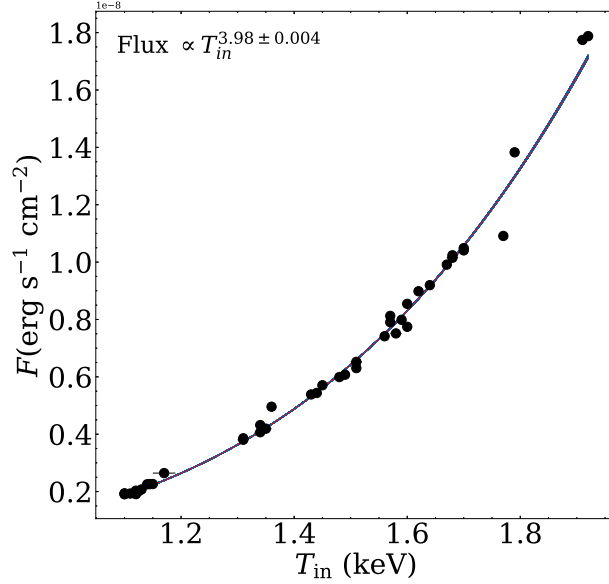


Figure 4. The disk unabsorbed flux (1–100 keV) versus the disk inner temperature (T_{in}). Flux is found to correlate with temperature in the form of proportional $T_{\text{in}}^{3.98}$

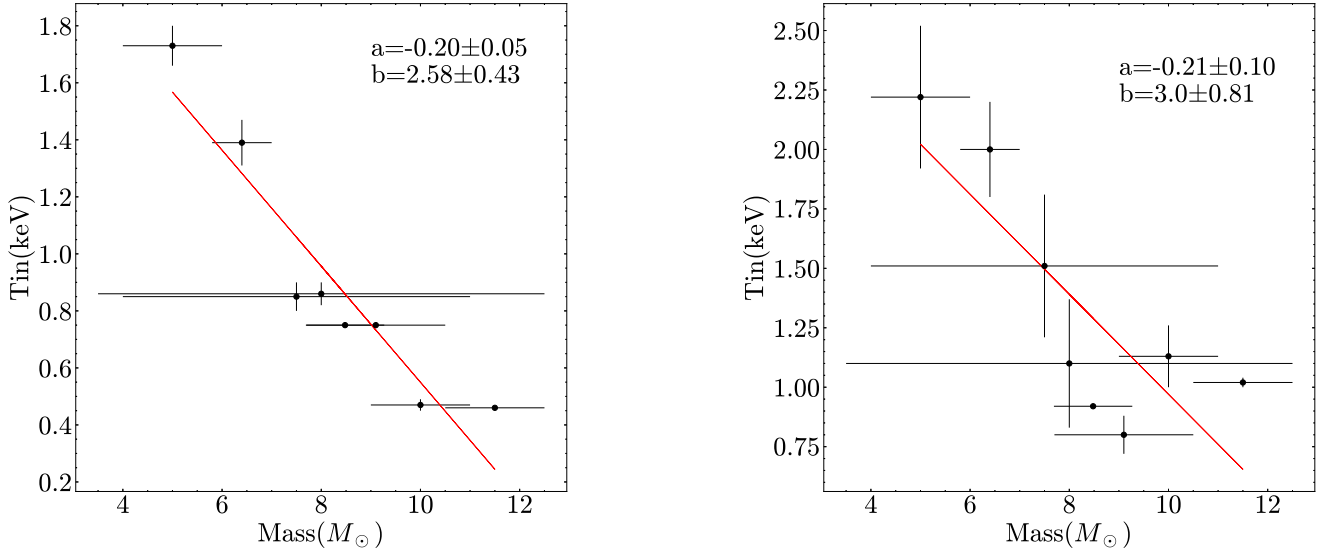


Figure 5. The relationship between the mass of a black hole and the maximum temperature of the inner disk in the soft state. Left panel: The observed maximum temperature of the inner disk in the soft state. For different maximum temperatures of disks with different outbursts of BHXRBS, we took the mean value. Right panel: Estimated temperature of the inner disk at a luminosity of $0.3 L_{\text{Edd}}$

disk temperature in soft state and black mass. As shown in the left panel of Figure 5, the two parameters of the disk temperature and the black hole mass have an anti-correlation, and a linear fit using Linmix (Kelly 2007) takes an empirical relation of $T_{\text{in}} = -0.20^{+0.05}_{-0.05}M + 2.58^{+0.43}_{-0.43}$. For SLX 1746–331, the maximum temperature of the inner disk is found to be $T_{\text{in}} = 1.9$ keV, and according to the above empirical relation, a measurement of disk temperature of 1.9 keV would result in an estimation of the compact object mass of $3.4 \pm 2.3 M_{\odot}$. Again, by assuming the outburst peak flux of $0.3 L_{\text{Edd}}$ and a compact mass of $3.3 \pm 2.3 M_{\odot}$, $\cos\theta$ is constrained as 0.96 ± 0.9 . Thus the inclination angle θ can be constrained as $0-84^{\circ}$.

For continuum fitting (CF) measurements of spin, it is essential for the accretion disk to extend up to the ISCO (Zhang et al. 1997; Li et al. 2005). Typically, the soft state with a disk luminosity $L_{\text{disk}} \leq 0.3 L_{\text{Edd}}$ is selected for

Table 4. The mass of a black hole X-ray binary and the maximum temperature of its inner disk in the soft state.

Sources	Mass M_{\odot}	Spin a	T_{in}^a keV	T_{in}^b keV	References
MAXI J1348–630	$9.1^{+1.6}_{-1.2}$	$0.78^{+0.04}_{-0.04}$	$0.75^{+0.01}_{-0.01}$	$0.80^{+0.08}_{-0.06}$	1,2,3
MAXI J1803–298	3.5–12.5	$0.991^{+0.001}_{-0.001}$	$0.86^{+0.04}_{-0.04}$	$1.10^{+0.27}_{-0.27}$	4,5
GRS 1758–258	≈ 10	$0.97^{+0.02}_{-0.05}$	$0.47^{+0.02}_{-0.02}$	$1.13^{+0.13}_{-0.13}$	6,7,8
MAXI J1727–203	≥ 11.5	$0.986^{+0.012}_{-0.159}$	$0.46^{+0.001}_{-0.001}$	$1.02^{+0.02}_{-0.02}$	9,10
4U 1957+11	5^{+1}_{-1}	$0.95^{+0.02}_{-0.04}$	$1.73^{+0.07}_{-0.07}$	$2.22^{+0.3}_{-0.3}$	10,11,12
V4641 Sgr	$6.4^{+0.6}_{-0.6}$	$0.86^{+0.02}_{-0.02}$	$1.39^{+0.03}_{-0.13}$	$2.0^{+0.3}_{-0.3}$	10,13
H 1743–322	$11.21^{+1.65}_{-1.96}$	$0.98^{+0.01}_{-0.02}$	$0.70^{+0.10}_{-0.14}$	$1.06^{+0.16}_{-0.17}$	10,14,15,16
MAXI J1820+070	$8.48^{+0.79}_{-0.79}$	$0.988^{+0.006}_{-0.028}$	$0.75^{+0.01}_{-0.01}$	$0.92^{+0.01}_{-0.01}$	17,18
GX 339–4	4–11	$0.95^{+0.02}_{-0.08}$	$0.85^{+0.03}_{-0.12}$	$1.5^{+0.3}_{-0.3}$	19,20

NOTE:

^a The maximum temperature of the inner disk in the soft state. The average value is taken for those with multiple outbursts.

^b Estimated inner disk temperatures for $0.3 L_{\text{Edd}}$

References. (1) Jana et al. (2020), (2) Jia et al. (2022), (3) Dai et al. (2023), (4) Jana et al. (2022b), (5) Feng et al. (2022), (6) Jana et al. (2022a), (7) Soria et al. (2011), (8) Smith et al. (2001), (9) Wang et al. (2022), (10) Draghis et al. (2023), (11) Sharma et al. (2021), (12) Nowak et al. (2008), (13) MacDonald et al. (2014), (14) Molla et al. (2017), (15) Cadolle Bel et al. (2004), (16) McClintock et al. (2009), (17) Torres et al. (2020), (18) Peng et al. (2023), (19) Shui et al. (2021), (20) Zdziarski et al. (2019)

Table 5. Fitting results with M3, where D , θ , and a represent the distance, inclination angle, and spin of the compact object, respectively. The spin of the compact object is derived via M3 fitting under the different parameter sets of D , mass, and θ .

$M = 3.4M_{\odot}$		$M = 5.7M_{\odot}$	
$D=7.29$ kpc	$\theta = 70^{\circ}, a=0.80^{+0.01}_{-0.01}$	$\theta = 84^{\circ}, a=0.86^{+0.02}_{-0.04}$	
$D=10.81$ kpc	$\theta = 16^{\circ}, a=0.93^{+0.02}_{-0.03}$	$\theta = 55^{\circ}, a=0.99^{+0.001}_{-0.04}$	
$D = 14.33$ kpc	$\theta = 0^{\circ}, a = 0.99^{+0.001}_{-0.01}$	$\theta = 18^{\circ}, a = 0.99^{+0.01}_{-0.01}$	

this purpose (Shakura & Sunyaev 1973; Novikov & Thorne 1973). In order to measure the spin of SLX 1746–331, we replace DISKBB model in M2 with KERRBB model and convolve it with THCOMP. Therefore, our new model M3 is CONSTANT*TBABS(THCOMP*KERRBB). The interstellar absorption is set to a fixed value of $0.64 \times 10^{22} \text{ cm}^{-2}$ based on the *NICER* fit. The electron temperature is also fixed at 150 keV. As shown in Table 5, since the range of inclination angles is relatively large, we choose a few sets for typical parameters of compact star mass, the source distance, and the inclination angle. These parameters are fixed separately in the M3. Additionally, the normalization of KERRBB is fixed at 1.0 in accordance with the requirements of the model. As shown in Table 5, all fitting results suggest that SLX 1746–331 hosts a compact object with a relatively high spin value (larger than 0.8).

For different BXRBs, the luminosities achieved in each outburst of the soft state are not the same, leading to systematic uncertainties in estimating the empirical relations addressed above. By assuming a peak flux of $0.3 L_{\text{Edd}}$ for each source, the disk temperatures are revised according to the formula $L_{\text{disk}} \approx 4\pi R_{\text{in}}^2 \sigma T_{\text{in}}^4$, and shown in Table 4, a linear fit to the revised disk temperature against the black hole mass results in empirical relations of $T_{\text{in}} = -0.21^{+0.1}_{-0.1} M + 2.0^{+0.81}_{-0.81}$. With this updated relationship, the mass of the compact object of SLX 1746–331 is revised as $5.2 \pm 4.5 M_{\odot}$. Again, a low-mass compact is suggested but with a larger uncertainty.

4. DISCUSSION AND CONCLUSION

We have carried out spectral analysis of the 2023 outburst of SLX 1746–331, which was observed thoroughly by *Insight*-HXMT and *NICER*. Our results reveal for the first time the possible properties of both the outburst and the compact object harbored within this system. The outburst manifested itself as an unusual evolution behavior that stayed mostly in the soft state, with an inner disk remaining around ISCO. The compact object mass is consistently estimated with different manners: a lower limit of $3.28 \pm 2.14 M_{\odot}$ by assuming $0.3 L_{\text{Edd}}$ of the outburst peak flux, and $5.2 \pm 4.5 M_{\odot}$ from the empirical correlation between disk temperature and black hole mass, established from a sample of black hole systems.

The previous observations on SLX 1746–331 with RXTE/PCA and INTEGRAL/JEM-X have already pointed to a transition nature and its soft spectrum, which is very similar to the soft state of a black hole, and thus it was identified as a black hole transient X-ray binary (Skinner et al. 1990; White & van Paradijs 1996; Homan & Wijnands 2003). The distance was estimated by Yan & Yu (2015) to be 10.81 ± 3.52 kpc using RXTE data, but the basic parameters of black hole mass and inclination of the system are still missing. When fitting the empirical relation, uncertainties are propagated to the final measurement of the black hole mass, resulting in a wider range of black hole mass. However, by incorporating the black hole mass obtained from the range of Eddington luminosities, we can place a constraint on the black hole mass of SLX 1746–331. Obviously, given the current outburst behavior of SLX 1746–331, a more constrained lower limit on the compact object can be derived if the source distance could be better measured in the future, and the mass can be directly estimated if an inclination angle could be available.

With the thorough observations of *Insight*-HXMT and *NICER*, the outburst of SLX 1746–331 is found with rather peculiar evolution behavior. The outburst was dominated by soft emission and the inner disk remained at ISCO during the almost entire outburst. Such behavior is rather different from the normal outburst experienced by the outburst of the black hole systems, which usually have a low hard state and intermediate state. Although rare, a similar outburst was also found in another black hole system MAXI J0637–430. Like SLX 1746–331, MAXI J0637–430 shows an outburst that lacks the hard state during the rising phase and directly transitions to the soft state (Ma et al. 2022). Therefore, SLX 1746–331 and MAXI J0637–430 may constitute a special sample of the black hole X-ray binary system with less prominent hard and intermediate states in their outbursts.

A comparison between SLX 1746–331 and MAXI J0637–430 shows the possible common feature in the mass of their compact object. Soria et al. (2022) estimate the black hole mass of MAXI J0637–430 to be about $5.1 \pm 1.6 M_{\odot}$, while the mass of the compact object (most likely a black hole) hosted in SLX 1746–331 is measured around $5.2 \pm 4.5 M_{\odot}$. However, these two systems are distinct in other aspects: MAXI J0637–430 hosts a low-spin (less than 0.25) black hole, underwent an outburst of less than $0.1 L_{\text{Edd}}$ peak luminosity and a maximum disk temperature of 0.7 keV; while SLX 1746–331 harbors a compact object with the relatively high spin of larger than 0.8 and is observed with a disk temperature of as high as 1.9 keV. MAXI J0637–430 has a donor star with a mass of $0.25 \pm 0.07 M_{\odot}$ and the shortest binary period $P_{\text{orb}} \approx 2.2_{-0.6}^{+0.8}$ hr (Ma et al. 2022; Soria et al. 2022), while for SLX 1746–331 the mass of the donor star and the orbital period are yet unknown. Both systems underwent outbursts without experiencing a clear hard state, which means that the transition from hard to soft states, if any, should have occurred at low accretion rates. State transition from hard to soft states has been addressed in Cao et al. (2021), where they think the critical accretion rate for state transition from hard to soft could be highly related to the large-scale magnetic field born out of the disk. The transition is balanced between the timescales of ion-electron equilibration and accretion of the ADAF. Note that the dependence of the disk magnetic field is positive for the former and negative for the latter, a transition to the soft state under a lower accretion rate in principle needs a low disk magnetic field. Since the disk is formed from matter accreted from the companion via Roche-Lobe, a system with a small compact object and tight orbital period could in principle result in a smaller accretion disk, and hence a weaker large-scale disk magnetic field. Therefore, the similar outburst behavior of SLX 1746–331 and MAXI J0637–430 might suggest both sources have small orbits and light compact objects, which are already confirmed for MAXI J0637–430. Furthermore, the compact object mass as measured in these two systems most likely falls into the long-debated mass gap of $3\text{--}5 M_{\odot}$ of the black holes, which makes them interesting observational targets for future observations by e.g., *Einstein Probe* (*EP*) (Yuan et al. 2018). Capturing the initial rising phase of the outbursts by *EP* would tell us if for such systems the low hard state really exists, as well the luminosity level for transition to the soft state.

1 This work is supported by the National Key R&D Program of China (2021YFA0718500), the National Natural Science
 2 Foundation of China under grants U1838201, U1838202, U2038101, U1938103, 12273030, U1938107. This work made
 3 use of data and software from the *Insight*-HXMT mission, a project funded by China National Space Administration
 4 (CNSA) and the Chinese Academy of Sciences(CAS). This work was partially supported by International Partnership
 5 Program of Chinese Academy of Sciences (Grant No.113111KYSB20190020). This research has made use of software
 6 provided by of data obtained from the High Energy Astrophysics Science Archive Research Center (HEASARC),
 7 provided by NASA's Goddard Space Flight Center. L. D. Kong is grateful for the financial support provided by the
 8 Sino-German (CSC-DAAD) Postdoc Scholarship Program (57251553).

REFERENCES

- Baby, B. E., Agrawal, V. K., Ramadevi, M. C., et al. 2020, MNRAS, 497, 1197, doi: [10.1093/mnras/staa1965](https://doi.org/10.1093/mnras/staa1965)
- Belloni, T., & Hasinger, G. 1990, A&A, 230, 103
- Belloni, T., Homan, J., Casella, P., et al. 2005, A&A, 440, 207, doi: [10.1051/0004-6361:20042457](https://doi.org/10.1051/0004-6361:20042457)
- Belloni, T. M., & Motta, S. E. 2016, in Astrophysics and Space Science Library, Vol. 440, Astrophysics of Black Holes: From Fundamental Aspects to Latest Developments, ed. C. Bambi, 61, doi: [10.1007/978-3-662-52859-4_2](https://doi.org/10.1007/978-3-662-52859-4_2)
- Belloni, T. M., Motta, S. E., & Muñoz-Darias, T. 2011, Bulletin of the Astronomical Society of India, 39, 409, doi: [10.48550/arXiv.1109.3388](https://doi.org/10.48550/arXiv.1109.3388)
- Brocksopp, C., Bandyopadhyay, R. M., & Fender, R. P. 2004, NewA, 9, 249, doi: [10.1016/j.newast.2003.11.002](https://doi.org/10.1016/j.newast.2003.11.002)
- Cadolle Bel, M., Rodriguez, J., Sizun, P., et al. 2004, A&A, 426, 659, doi: [10.1051/0004-6361:20041292](https://doi.org/10.1051/0004-6361:20041292)
- Cannizzo, J. K., Chen, W., & Livio, M. 1995, ApJ, 454, 880, doi: [10.1086/176541](https://doi.org/10.1086/176541)
- Cao, X., You, B., & Yan, Z. 2021, A&A, 654, A81, doi: [10.1051/0004-6361/202141652](https://doi.org/10.1051/0004-6361/202141652)
- Cao, X., Jiang, W., Meng, B., et al. 2020, Science China Physics, Mechanics, and Astronomy, 63, 249504, doi: [10.1007/s11433-019-1506-1](https://doi.org/10.1007/s11433-019-1506-1)
- Capitanio, F., Belloni, T., Del Santo, M., & Ubertini, P. 2009, MNRAS, 398, 1194, doi: [10.1111/j.1365-2966.2009.15196.x](https://doi.org/10.1111/j.1365-2966.2009.15196.x)
- Chen, Y., Cui, W., Li, W., et al. 2020, Science China Physics, Mechanics, and Astronomy, 63, 249505, doi: [10.1007/s11433-019-1469-5](https://doi.org/10.1007/s11433-019-1469-5)
- Corral-Santana, J. M., Casares, J., Muñoz-Darias, T., et al. 2016, A&A, 587, A61, doi: [10.1051/0004-6361/201527130](https://doi.org/10.1051/0004-6361/201527130)
- Dai, X., Kong, L., Bu, Q., et al. 2023, MNRAS, 521, 2692, doi: [10.1093/mnras/stad714](https://doi.org/10.1093/mnras/stad714)
- Deegan, P., Combet, C., & Wynn, G. A. 2009, MNRAS, 400, 1337, doi: [10.1111/j.1365-2966.2009.15573.x](https://doi.org/10.1111/j.1365-2966.2009.15573.x)
- Done, C., & Diaz Trigo, M. 2010, MNRAS, 407, 2287, doi: [10.1111/j.1365-2966.2010.17092.x](https://doi.org/10.1111/j.1365-2966.2010.17092.x)
- Draghis, P. A., Miller, J. M., Zoghbi, A., et al. 2023, ApJ, 946, 19, doi: [10.3847/1538-4357/acafe7](https://doi.org/10.3847/1538-4357/acafe7)
- Esin, A. A., McClintock, J. E., & Narayan, R. 1997, ApJ, 489, 865, doi: [10.1086/304829](https://doi.org/10.1086/304829)
- Fender, R. P., Belloni, T. M., & Gallo, E. 2004, MNRAS, 355, 1105, doi: [10.1111/j.1365-2966.2004.08384.x](https://doi.org/10.1111/j.1365-2966.2004.08384.x)
- Feng, Y., Zhao, X., Li, Y., et al. 2022, MNRAS, 516, 2074, doi: [10.1093/mnras/stac1868](https://doi.org/10.1093/mnras/stac1868)
- García, J. A., Steiner, J. F., McClintock, J. E., et al. 2015, ApJ, 813, 84, doi: [10.1088/0004-637X/813/2/84](https://doi.org/10.1088/0004-637X/813/2/84)
- Gendreau, K. C., Arzoumanian, Z., Adkins, P. W., et al. 2016, in Society of Photo-Optical Instrumentation Engineers (SPIE) Conference Series, Vol. 9905, Space Telescopes and Instrumentation 2016: Ultraviolet to Gamma Ray, ed. J.-W. A. den Herder, T. Takahashi, & M. Bautz, 99051H, doi: [10.1117/12.2231304](https://doi.org/10.1117/12.2231304)
- Gierliński, M., Done, C., & Page, K. 2008, MNRAS, 388, 753, doi: [10.1111/j.1365-2966.2008.13431.x](https://doi.org/10.1111/j.1365-2966.2008.13431.x)
- Hertz, P., & Grindlay, J. E. 1984, ApJ, 278, 137, doi: [10.1086/161775](https://doi.org/10.1086/161775)
- Homan, J., & Belloni, T. 2005, Ap&SS, 300, 107, doi: [10.1007/s10509-005-1197-4](https://doi.org/10.1007/s10509-005-1197-4)
- Homan, J., & Wijnands, R. 2003, The Astronomer's Telegram, 169, 1
- Homan, J., Wijnands, R., van der Klis, M., et al. 2001, ApJS, 132, 377, doi: [10.1086/318954](https://doi.org/10.1086/318954)
- Jana, A., Chang, H.-K., Chatterjee, A., Naik, S., & Safi-Harb, S. 2022a, ApJ, 936, 3, doi: [10.3847/1538-4357/ac84dd](https://doi.org/10.3847/1538-4357/ac84dd)
- Jana, A., Debnath, D., Chatterjee, D., et al. 2020, ApJ, 897, 3, doi: [10.3847/1538-4357/ab9696](https://doi.org/10.3847/1538-4357/ab9696)
- Jana, A., Naik, S., Jaisawal, G. K., et al. 2022b, MNRAS, 511, 3922, doi: [10.1093/mnras/stac315](https://doi.org/10.1093/mnras/stac315)
- Jia, N., Zhao, X., Gou, L., et al. 2022, MNRAS, 511, 3125, doi: [10.1093/mnras/stac121](https://doi.org/10.1093/mnras/stac121)
- Kelly, B. C. 2007, ApJ, 665, 1489, doi: [10.1086/519947](https://doi.org/10.1086/519947)
- Kuulkers, E., Beckmann, V., Shaw, S., et al. 2008, The Astronomer's Telegram, 1385, 1

- Lasota, J.-P. 2001, *NewAR*, 45, 449, doi: [10.1016/S1387-6473\(01\)00112-9](https://doi.org/10.1016/S1387-6473(01)00112-9)
- Li, L.-X., Zimmerman, E. R., Narayan, R., & McClintock, J. E. 2005, *ApJS*, 157, 335, doi: [10.1086/428089](https://doi.org/10.1086/428089)
- Liao, J.-Y., Zhang, S., Lu, X.-F., et al. 2020, *Journal of High Energy Astrophysics*, 27, 14, doi: [10.1016/j.jheap.2020.04.002](https://doi.org/10.1016/j.jheap.2020.04.002)
- Liu, C., Zhang, Y., Li, X., et al. 2020, *Science China Physics, Mechanics, and Astronomy*, 63, 249503, doi: [10.1007/s11433-019-1486-x](https://doi.org/10.1007/s11433-019-1486-x)
- Ma, R. C., Soria, R., Tao, L., et al. 2022, *MNRAS*, 514, 5238, doi: [10.1093/mnras/stac1585](https://doi.org/10.1093/mnras/stac1585)
- MacDonald, R. K. D., Bailyn, C. D., Buxton, M., et al. 2014, *ApJ*, 784, 2, doi: [10.1088/0004-637X/784/1/2](https://doi.org/10.1088/0004-637X/784/1/2)
- Markwardt, C. B., & Swank, J. H. 2007, *The Astronomer's Telegram*, 1235, 1
- McClintock, J. E., & Remillard, R. A. 2006, in *Compact stellar X-ray sources*, Vol. 39, 157–213, doi: [10.48550/arXiv.astro-ph/0306213](https://doi.org/10.48550/arXiv.astro-ph/0306213)
- McClintock, J. E., Remillard, R. A., Rupen, M. P., et al. 2009, *ApJ*, 698, 1398, doi: [10.1088/0004-637X/698/2/1398](https://doi.org/10.1088/0004-637X/698/2/1398)
- Miller, J. M., Homan, J., Steeghs, D., et al. 2006, *ApJ*, 653, 525, doi: [10.1086/508644](https://doi.org/10.1086/508644)
- Mitsuda, K., Inoue, H., Koyama, K., et al. 1984, *PASJ*, 36, 741
- Miyamoto, S., Kitamoto, S., Iga, S., Negoro, H., & Terada, K. 1992, *ApJL*, 391, L21, doi: [10.1086/186389](https://doi.org/10.1086/186389)
- Molla, A. A., Chakrabarti, S. K., Debnath, D., & Mondal, S. 2017, *ApJ*, 834, 88, doi: [10.3847/1538-4357/834/1/88](https://doi.org/10.3847/1538-4357/834/1/88)
- Motch, C., Guillout, P., Haberl, F., et al. 1998, *A&AS*, 132, 341, doi: [10.1051/aas:1998299](https://doi.org/10.1051/aas:1998299)
- Motta, S., Belloni, T., & Homan, J. 2009, *MNRAS*, 400, 1603, doi: [10.1111/j.1365-2966.2009.15566.x](https://doi.org/10.1111/j.1365-2966.2009.15566.x)
- Motta, S., Homan, J., Muñoz Darias, T., et al. 2012, *MNRAS*, 427, 595, doi: [10.1111/j.1365-2966.2012.22037.x](https://doi.org/10.1111/j.1365-2966.2012.22037.x)
- Novikov, I. D., & Thorne, K. S. 1973, in *Black Holes (Les Astres Occlus)*, 343–450
- Nowak, M. A., Juett, A., Homan, J., et al. 2008, *ApJ*, 689, 1199, doi: [10.1086/592227](https://doi.org/10.1086/592227)
- Ozawa, H., Suwa, F., Negoro, H., et al. 2011, *The Astronomer's Telegram*, 3098, 1
- Peng, J. Q., Zhang, S., Chen, Y. P., et al. 2023, *MNRAS*, 518, 2521, doi: [10.1093/mnras/stac3238](https://doi.org/10.1093/mnras/stac3238)
- Salvesen, G., Miller, J. M., Reis, R. C., & Begelman, M. C. 2013, *MNRAS*, 431, 3510, doi: [10.1093/mnras/stt436](https://doi.org/10.1093/mnras/stt436)
- Shakura, N. I., & Sunyaev, R. A. 1973, *A&A*, 24, 337
- Sharma, P., Sharma, R., Jain, C., Dewangan, G. C., & Dutta, A. 2021, *Research in Astronomy and Astrophysics*, 21, 214, doi: [10.1088/1674-4527/21/9/214](https://doi.org/10.1088/1674-4527/21/9/214)
- Shui, Q. C., Yin, H. X., Zhang, S., et al. 2021, *MNRAS*, 508, 287, doi: [10.1093/mnras/stab2521](https://doi.org/10.1093/mnras/stab2521)
- Skinner, G. K., Foster, A. J., Willmore, A. P., & Eyles, C. J. 1990, *MNRAS*, 243, 72, doi: [10.1093/mnras/243.1.72](https://doi.org/10.1093/mnras/243.1.72)
- Smith, D. M., Heindl, W. A., Markwardt, C. B., & Swank, J. H. 2001, *ApJL*, 554, L41, doi: [10.1086/320928](https://doi.org/10.1086/320928)
- Soria, R., Broderick, J. W., Hao, J., et al. 2011, *MNRAS*, 415, 410, doi: [10.1111/j.1365-2966.2011.18714.x](https://doi.org/10.1111/j.1365-2966.2011.18714.x)
- Soria, R., Ma, R., Tao, L., & Zhang, S.-N. 2022, *MNRAS*, 515, 3105, doi: [10.1093/mnras/stac1896](https://doi.org/10.1093/mnras/stac1896)
- Steiner, J. F., McClintock, J. E., Remillard, R. A., et al. 2010, *ApJL*, 718, L117, doi: [10.1088/2041-8205/718/2/L117](https://doi.org/10.1088/2041-8205/718/2/L117)
- Tetarenko, B. E., Sivakoff, G. R., Heinke, C. O., & Gladstone, J. C. 2016, *ApJS*, 222, 15, doi: [10.3847/0067-0049/222/2/15](https://doi.org/10.3847/0067-0049/222/2/15)
- Torres, M. A. P., Casares, J., Jiménez-Ibarra, F., et al. 2020, *ApJL*, 893, L37, doi: [10.3847/2041-8213/ab863a](https://doi.org/10.3847/2041-8213/ab863a)
- Verner, D. A., Ferland, G. J., Korista, K. T., & Yakovlev, D. G. 1996, *ApJ*, 465, 487, doi: [10.1086/177435](https://doi.org/10.1086/177435)
- Wang, S., Kawai, N., Shidatsu, M., et al. 2022, *MNRAS*, 514, 5320, doi: [10.1093/mnras/stac1503](https://doi.org/10.1093/mnras/stac1503)
- Warwick, R. S., Norton, A. J., Turner, M. J. L., Watson, M. G., & Willingale, R. 1988, *MNRAS*, 232, 551, doi: [10.1093/mnras/232.3.551](https://doi.org/10.1093/mnras/232.3.551)
- White, N. E., & van Paradijs, J. 1996, *ApJL*, 473, L25, doi: [10.1086/310380](https://doi.org/10.1086/310380)
- Wilms, J., Allen, A., & McCray, R. 2000, *ApJ*, 542, 914, doi: [10.1086/317016](https://doi.org/10.1086/317016)
- Wilson, C. A., Patel, S. K., Kouveliotou, C., et al. 2003, *ApJ*, 596, 1220, doi: [10.1086/377473](https://doi.org/10.1086/377473)
- Yan, Z., & Yu, W. 2015, *ApJ*, 805, 87, doi: [10.1088/0004-637X/805/2/87](https://doi.org/10.1088/0004-637X/805/2/87)
- Yuan, W., Zhang, C., Ling, Z., et al. 2018, in *Society of Photo-Optical Instrumentation Engineers (SPIE) Conference Series*, Vol. 10699, *Space Telescopes and Instrumentation 2018: Ultraviolet to Gamma Ray*, ed. J.-W. A. den Herder, S. Nikzad, & K. Nakazawa, 1069925, doi: [10.1117/12.2313358](https://doi.org/10.1117/12.2313358)
- Zdziarski, A. A., Ziłkowski, J., & Mikołajewska, J. 2019, *MNRAS*, 488, 1026, doi: [10.1093/mnras/stz1787](https://doi.org/10.1093/mnras/stz1787)
- Zhang, S., Lu, F. J., Zhang, S. N., & Li, T. P. 2014, in *Society of Photo-Optical Instrumentation Engineers (SPIE) Conference Series*, Vol. 9144, *Space Telescopes and Instrumentation 2014: Ultraviolet to Gamma Ray*, ed. T. Takahashi, J.-W. A. den Herder, & M. Bautz, 914421, doi: [10.1117/12.2054144](https://doi.org/10.1117/12.2054144)

- Zhang, S., Zhang, S. N., Lu, F. J., et al. 2018, in Society of Photo-Optical Instrumentation Engineers (SPIE) Conference Series, Vol. 10699, Space Telescopes and Instrumentation 2018: Ultraviolet to Gamma Ray, ed. J.-W. A. den Herder, S. Nikzad, & K. Nakazawa, 106991U, doi: [10.1117/12.2311835](https://doi.org/10.1117/12.2311835)
- Zhang, S. N., Cui, W., & Chen, W. 1997, ApJL, 482, L155, doi: [10.1086/310705](https://doi.org/10.1086/310705)
- Zhang, S.-N., Li, T., Lu, F., et al. 2020, Science China Physics, Mechanics, and Astronomy, 63, 249502, doi: [10.1007/s11433-019-1432-6](https://doi.org/10.1007/s11433-019-1432-6)